

This is the accepted manuscript made available via CHORUS. The article has been published as:

Anomalous nanoclusters, anisotropy, and electronic nematicity in the doped manganite

$\text{La}_{\{1/3\}}\text{Ca}_{\{2/3\}}\text{MnO}_{\{3\}}$

J. Tao, K. Sun, J. M. Tranquada, and Y. Zhu

Phys. Rev. B **95**, 235113 — Published 7 June 2017

DOI: [10.1103/PhysRevB.95.235113](https://doi.org/10.1103/PhysRevB.95.235113)

Anomalous nanoclusters, anisotropy and electronic nematicity in doped manganite  
 $\text{La}_{1/3}\text{Ca}_{2/3}\text{MnO}_3$

J. Tao<sup>1,\*</sup>, K. Sun<sup>2</sup>, J. M. Tranquada<sup>1</sup> and Y. Zhu<sup>1</sup>

<sup>1</sup>Condensed Matter Physics & Materials Science Department, Brookhaven National Laboratory,  
Upton, NY 11973

<sup>2</sup>Department of Physics, University of Michigan, Ann Arbor, MI 48109

\* [jtao@bnl.gov](mailto:jtao@bnl.gov)

## Abstract

In doped manganites, a superlattice modulation associated with charge/orbital ordering is accepted as a key component in understanding many intriguing properties. It has been reported that the superlattice modulation always appears on the  $a$ -axis of the crystals. Here, by using multiple transmission electron microscopic techniques, we observe a type of anomalous nanoclusters in which the superlattice modulation appears on the  $c$ -axis of  $\text{La}_{1/3}\text{Ca}_{2/3}\text{MnO}_3$ . By correlating the thermal evolution of the anomalous nanoclusters to other property measurements, we suggest that strain is responsible for the formation of the anomalous nanoclusters. The phase separation and phase transition scenario in  $\text{La}_{1/3}\text{Ca}_{2/3}\text{MnO}_3$  are also described using electronic-liquid-crystal (ELC) phases. An ELC phase diagram in  $\text{La}_{1/3}\text{Ca}_{2/3}\text{MnO}_3$  is constructed as a function of temperature based on our observations.

## Introduction

In strongly-correlated systems, it has long been known that spatial modulations of charge, orbital or spin can arise and couple to the lattice, playing a crucial role in materials' functionality. Many experimental techniques were employed to study those electronic modulations to understand the underlying physics. In general, the electronic modulations or structures can be probed globally by using volume averaged probes, e.g. neutron, x-ray and electron scatterings techniques, or locally by using spatially confined probes, e.g., scanning tunneling microscopy (STM) and transmission electron microscopy (TEM). The interpretation of the results depends on the strength of each technique and different techniques may reveal the characteristics of the electronic structure/modulation from different aspects. For instance, global probes provide accurate characterizations of long-range (LR) electronic ordering, while local probes detect short-range (SR) modulations with high spatial resolution, even in the absence of LR ordering.

In our previous work [1], we demonstrated a study of electronic phase transitions in a doped manganite  $\text{La}_{1/3}\text{Ca}_{2/3}\text{MnO}_3$ , where a superlattice modulation develops during cooling from the temperature  $\sim 310$  K- slightly above room temperature. This superlattice structure is often associated to charge-ordering (CO) and/or orbital-ordering (OO) in the electronic structures [2, 3]. To solve the controversial discussions about the CO/OO transition temperatures and the origin of incommensurability measured from the CO/OO structures [4-7], we performed a temperature-dependent TEM study and obtained results in real-space, reciprocal-space and energy-space. Our findings, using electron local probes, evidently show that charge segregation plays a key role in the formation of incommensurate SR structures [1]. In the characterization of the CO/OO phase transitions, the symmetry descriptions developed in the area of electronic-liquid-crystal (ELC) phases were found to be helpful in distinguishing SR phases and identifying

the role of electronic defects in the LR-SR transitions. Despite the fact that the crystal structure of  $\text{La}_{1/3}\text{Ca}_{2/3}\text{MnO}_3$  has some anisotropy (orthorhombic; see Ref. 3) at 310 K, there is no superlattice structure at this temperature and, therefore, the electronic structure can be considered as an isotropic phase. Upon cooling, the superlattice modulation appears along the  $a$ -axis (i.e. being unidirectional) in the form of a SR stripe phase, i. e., being electronic nematic in the bulk material from symmetry description. The superlattice structure remains SR in the temperature range from 310 K down to 220 K. Below 220 K, the superlattice structure becomes LR and an electronic smectic in the bulk material. Our previous work provided the microscopic characterization from electronic smectic-nematic and nematic-isotropic transitions [1], however, it did not correlate the ELC phase transitions to the lattice constant variation and other property measurements in  $\text{La}_{1/3}\text{Ca}_{2/3}\text{MnO}_3$ .

On the other hand, the experimental observations in doped manganites provide a new playground for the development of the ELC phases. Recently SR electronic structures, which are sometimes viewed as electronic phase separations in the static cases, attract particular attention for the study of disorder effects in correlated materials [8-11]. The competition between LR and SR electronic modulations give rise to interesting phenomena, which is generally described in the classification of ELC phases. For example, an unidirectional charge/orbital/spin modulation with fixed wavelength can be characterized by two quantities, the orientation of wavevector in the crystal and the phase of modulation wave, and, in general, three possible quantum phases can emerge as follows [12, 13]. (1) Both the orientation and phase develop LR ordering. Such a state will result in sharp peaks in scattering experiments, indicating large coherent length in real space. This state, at macroscopic scales, breaks the lattice rotational symmetry and translational symmetry along one direction. In analogy to a smectic state in liquid crystals, the electronic

modulation having long-range ordering of both orientation and phase is referred to as an electronic smectic state. (2) The orientation of the wavevector develops LR correlation, but the phase shows strong inhomogeneity. The key signature of this state is *the anisotropy in the absence of LR spatial modulations*. This anisotropy may be associated with the change in lattice constants, transport properties, etc. Due to the absence of LR phase coherence, scattering experiments obtained from such a phase show broad bumps, instead of sharp peaks. Local probes will observe domains of SR spatial modulations at the same orientation with respect to the lattice. However, the phase of the modulation varies from one domain to another. At macroscopic scales, this state only breaks the lattice rotational symmetry (i.e., anisotropy), and, thus, is known as the electronic nematic phase. (3) If neither the orientation nor the phase develops LR coherence, the system is in a disordered (isotropic) phase, where anisotropy signals vanish. There are two subcases under this category. The electronic modulation on top of the crystal structure may completely disappear, even locally. No scattering signal can be detected from electronic modulations in addition to the fundamental lattice reflections. However, in several materials with reported observations of the ELC phases, the lattice constants of at least two orientations are very close. In such case, local probes may observe domains, where the orientations of the modulations distribute along different directions with equal probability in electronic isotropic phase. Scattering experiments may show broad pumps with equal intensity along different directions.

The observation and the characterization of the above ELC states are of great significance since the formation and evolution of the ELC phases have been accepted as the central mechanisms in many correlated materials [12-19]. However, the characterization of the ELC phases has been limited by the technical methods and the material systems. Some key observations of the ELC phases during the phase transitions are still lacking. Particularly, for

incommensurate electronic modulations, disorder effects destabilize smectic states and only nematic states appear in 2D systems, which are the suitable materials for STM observations. Comprehensive observations are needed to cover both the SR and LR (for both wave-vector orientation and phase) electronic modulations with their evolution through the ELC phase transitions and those observations should be correlated to materials' property measurements. Concepts, such as anisotropy and nematicity, have, at times, been used with confusion and should be clarified by the observations.

## **Results and Discussion**

Here, we report our continuous work on  $\text{La}_{1/3}\text{Ca}_{2/3}\text{MnO}_3$  with a discovery of anomalous nanoclusters in the electronic nematic phase. The anomalous nanoclusters have the SR superlattice structure along the  $c$ -axis (with the lattice constant very close to that along the  $a$ -axis), coexisting with nanoclusters having the SR superlattice structures along the  $a$ -axis in a phase separation scenario within the temperature range of 245 K to 310 K. We obtained direct observations of both types of nanoclusters, in real-space and in reciprocal space, as a function of temperature. After correlating the appearance of the anomalous nanoclusters with lattice variation through the phase transitions, our findings strongly suggest that the anomalous nanoclusters are directly related to the lattice variation and the abrupt change in heat capacity. The wavevector measured from the anomalous nanoclusters has a distinct temperature-dependent behavior compared with the normal nanoclusters (SR superlattice structure along  $a$ -axis). The formation of the anomalous nanoclusters might be a result of strain effects. Finally, we constructed an ELC phase diagram with all the observed phenomena during the ELC phase transitions and proposed the origin of the ELC phase transitions in  $\text{La}_{1/3}\text{Ca}_{2/3}\text{MnO}_3$ .

Material synthesis and the crystal structure of polycrystalline  $\text{La}_{1/3}\text{Ca}_{2/3}\text{MnO}_3$  can be found in our previous work [20]. Unlike the previously reported results that the superlattice reflections (SLRs) always appear along the  $a$ -axis [2, 3, 20], the electron diffraction and the dark-field TEM image (see Ref. 1 and 6 for the imaging condition) obtained from a single-crystal domain in Fig. 1 clearly show the SLRs along both the  $a$ -axis and the  $c$ -axis at the temperature  $\sim 280$  K. We ruled out the possibility of a superposition of two orthogonal crystalline domains in the projection in our observed areas because LR unidirectional superlattice structure was observed to be along the  $a$ -axis only in the same area at temperatures lower than 220 K. The superlattice structures can be seen, from the dark-field TEM image, to form in local areas of a few nanometers in extent, with SR stripes arranged along either the  $a$ -axis or the  $c$ -axis. The observation of the anomalous nanoclusters with the superlattice on the  $c$ -axis is typical in the  $\text{La}_{1/3}\text{Ca}_{2/3}\text{MnO}_3$  sample. The appearance of the anomalous nanoclusters is unexpected in this manganite and could provide additional insight into the understanding of the ELC phases.

We further obtained temperature-dependent observations of the anomalous nanoclusters in order to reveal their thermal evolution. It is challenging to achieve such observations with quantitative analysis by using dark-field TEM images because the contrast of the dark-field TEM images gets weaker as the temperature increases. Therefore, we used the scanning electron nanodiffraction (SEND) imaging technique [20], which has both the sensitivity on detecting the SLRs in the reciprocal space and resolution of mapping SLRs in real-space. Two typical electron nanodiffraction patterns during the scanning of the electron probe are shown in the Fig. 2a) and 2b), indicating the local superlattice structures along either the  $a$ -axis or the  $c$ -axis. The real-space distribution and the thermal evolution of the anomalous nanoclusters are clearly visualized in Fig. 2c) during a warming process, demonstrated by the purple nanoclusters (superstructure on

the  $c$ -axis) in the maps. In addition, the SR superstructure along the  $a$ -axis appears in red nanoclusters (normal nanoclusters) and no superstructure in the blue region. At the temperature below  $T \sim 245$  K, there is no anomalous nanocluster observed. The anomalous nanoclusters remain at nominally the same size at temperatures higher than  $T \sim 245$  K and its density seems to peak at  $T \sim 280$  K. At room temperature, both the normal (red) and anomalous (purple) nanoclusters are small in size and rare in population in the scanned area, until they fully disappear at  $T \sim 310$  K.

The formation and thermal evolution of the anomalous nanoclusters are distinct from that of the normal nanoclusters in this material on a number of aspects. The normal nanoclusters formed at  $T \sim 210$  K when the system becomes electronic phase separated [1]. Such temperature is much lower than the formation temperature of the anomalous nanoclusters. Upon warming, the normal nanoclusters shrink in size, while the size of the anomalous nanoclusters remains constant at  $\sim 3$ -4 nm in diameter until they disappear. Beyond those differences, the wavenumber measured from the anomalous nanoclusters behaves differently as a function of temperature from the normal nanoclusters. Shown in Fig. 3a), the measurements of the wavenumber have relatively small changes during a warming process at incommensurate values. Note that the wavenumber of the SLRs was measured by using both the coherent electron diffraction patterns obtained from a large area and electron nanodiffraction during the scanning with a nanometer-sized electron probe, with consistency between the two measurements. Although the intensities from the SLRs in the anomalous nanoclusters are much weaker such that the uncertainty of the measurements is larger than those measured from normal nanoclusters, it is evident that the thermal evolution of the wavenumber is distinct between the two types of nanoclusters, in addition to their formation temperature and their size variation through the thermal process.

The divergent behavior of the two types of nanoclusters suggests that the driving forces behind the two nanoclusters' formation are different. We propose here that the strain in the crystal lattice can be the driving force of the formation of the anomalous nanoclusters. Previous work has demonstrated that strain may cause the phase separation scenario that is similar to what we observed here, i.e., the separation of two phases with order parameters along perpendicular directions in crystals having the pseudocubic lattice [21]. Moreover, we noticed that the formation temperature of the anomalous nanoclusters coincides with the lattice variation temperature measured using both synchrotron x-ray and neutron scattering techniques in the same material at the same doping level [3, 22]. Since the lattice response in doped manganites is sensitive to the influence of a number of degrees of freedom such as orbital, charge and spin [1-11, 22], other mechanisms including chemical inhomogeneities may be responsible for the anomalous nanoclusters as well. Without sufficient evidence, it is beyond the scope of this work to pinpoint the driving mechanism here. In order to quantify the behaviors of the two types of nanoclusters so that we can correlate their behaviors to other structural and property measurements such as the lattice variation, we measured the anisotropy of the superstructures with two perpendicular order parameters in the bulk material. We used the definition and the method of measuring anisotropy in the case of  $\text{Bi}_2\text{Sr}_2\text{CaCu}_2\text{O}_{8+\delta}$  [23] for the observed electronic nematic phase having a strikingly similar phase separation as we observed in  $\text{La}_{1/3}\text{Ca}_{2/3}\text{MnO}_3$ . The anisotropy is defined by  $(I_a - I_c)/(I_a + I_c)$ , where  $I_a$  and  $I_c$  are the intensities of the SLRs on the  $a$ -axis and  $c$ -axis, respectively. In the isotropic phase, both the  $I_a$  and  $I_c$  are zero such that the anisotropy of the electronic structure in the bulk equals to zero. At the temperatures lower than the formation temperature of the anomalous nanoclusters,  $I_c$  is zero such that the anisotropy equals to one. The anisotropy measurements as a function of temperature are plotted in Fig. 3b

with a correlation to the lattice constant measurements from neutron scattering [22]. It can be clearly seen that the change of the anisotropy takes place at the same temperature range as the lattice constant variation at  $245 \text{ K} \leq T \leq 310 \text{ K}$ .

Given the fact that the crystalline symmetry of  $\text{La}_{1/3}\text{Ca}_{2/3}\text{MnO}_3$  is already changed from cubic to orthorhombic at 1100 K [24], it is important to identify the origin of the anisotropy, i.e. whether the main driving force for the anisotropy comes from electrons or the lattice background. The subtleties to distinguish lattice anisotropy from correlated electronic effects have been understood in the study of nematicity in de-twinned  $\text{YBa}_2\text{Cu}_3\text{O}_{6+x}$  single crystals, which also has an orthorhombic lattice [15, 25]. Similar as in  $\text{YBa}_2\text{Cu}_3\text{O}_{6+x}$ , here, the rapid rise of anisotropy near 310K upon cooling strongly indicates that this anisotropy is electronically driven, while the variation of lattice constants in this temperature range [22] is a result of the electronic structural intricacies. The change in structural anisotropy is too large to result from any mechanism driven only by the lattice. The emergence of the anomalous nanoclusters arises from the local strain variation and is responsible for the anisotropy measurements in Fig. 3b), which could explain the coincidence between the anisotropy measurements and the lattice constants. Moreover, the abrupt appearance of the anomalous nanoclusters gives rise to the sharp response in the specific heat measurement at  $T \sim 245 \text{ K}$  reported by the previous work on the same material at the same doping level [22]. This temperature was sometimes characterized as the transition temperature for the CO/OO superlattice structure in this material [22]. However, with the observations and characterizations here, it is clear that this temperature is neither the electronic smectic-nematic transition temperature nor the electronic nematic-isotropic transition temperature, but in the middle of the electronic nematic phase where the anomalous nanoclusters start to appear, indicating the strong influence of the anomalous nanoclusters in the entropy of the structure.

Finally, the volume fraction of the nanoclusters (both types included) was estimated as a function of temperature, shown in the inset of Fig. 3a), using the following method. The sample thickness was estimated to be  $\sim 10\text{-}20$  nm in the scanning area in the SEND maps in Fig. 2c). Assuming that the nano-phases have an isotropic shape in 3D and there is no overlapping of the nanoclusters through the sample thickness, the volume fraction can be derived from the SEND maps within a few percent. We note that the volume fraction becomes significant small at  $T \sim 280$  K during the warming process. This temperature coincides with the temperature when an abrupt decrease in electrical resistivity takes place upon warming [22] in the same material. Such observation indicates that the formation of insulating nanoclusters have a direct effect on the electrical transport properties.

## Summary

To summarize, we constructed an ELC phase diagram of  $\text{La}_{1/3}\text{Ca}_{2/3}\text{MnO}_3$  together with part of the findings from the previous work [1], as shown in Fig 4. An electronic smectic-nematic-isotropic phase transition was characterized by microscopic observations. It was observed that individual defects in the superstructure cannot break the LR symmetry and, thus, are not responsible for the smectic-nematic phase transition. Indeed, the appearance of electronic phase separation was observed to truly break the LR phase coherency into SR and cause the smectic-nematic transition via the proliferation of the defects in the superstructure. The proposed driving force of the smectic-nematic transition is charge segregation suggested by the previous findings [1, 26]. The electronic nematic phase is divided by two parts based on our observations. During a warming up process, the electronic modulation (i.e., superlattice structure) first breaks into normal nanoclusters (SLRs as broad bumps along the  $a$ -axis) separated by disordered regions. At this stage, the orientation of the wavevector is LR and unidirectional but the phase

has SR coherence spatially. Therefore, the material is globally electronic nematic. At a temperature higher than the smectic-nematic phase transition, i. e.,  $\sim 245$  K in  $\text{La}_{1/3}\text{Ca}_{2/3}\text{MnO}_3$ , anomalous nanoclusters with the superstructure on an orthogonal orientation (the  $c$ -axis) emerge from the disorder area. The wavevector of the electronic modulation is not unidirectional and the phase has SR coherence. The intensities of the SLRs along the  $a$ -axis and the  $c$ -axis are highly unequal; namely the density and the size of the normal nanoclusters and the anomalous nanoclusters are distinct in real-space. Therefore, the electronic modulation is still globally electronic nematic until both types of nanoclusters disappear at 310 K where the systems becomes electronic isotropic. We note that the volume fraction of the nanoclusters has an abrupt decrease at 280 K to small values and continues decreasing until they are undetectable at 310 K. Therefore, the nematic-isotropic phase transition takes place in this highly doped material in the temperature regime from 280 K to 310 K. We emphasize that electronic nematic regime in this material cannot be fully determined by the anisotropy measurements using intensities on the two orientations. In the electronic nematic regime without anomalous nanoclusters, the anisotropy is equal to one which is the same as in the electronic smectic phase; the material is nevertheless *anisotropic in the absence of LR spatial modulations* at the global scale and, therefore, is still electronic nematic. This observation should get attention by the community using various techniques for the characterization of ELC phases. The temperature-dependent behavior of the anisotropy of the superstructure coincides with the variation of lattice constants, which is within the nematic phase regime. Our results suggest that both charge segregation (see Ref. 1) and strain can be the possible driving mechanisms of the nematic-isotropic phase transition.

## **Acknowledgment**

We thank Dr. Maria Teresa Fernandez-Diaz for providing the published results of the lattice constants. This research is sponsored by the US Department of Energy (DOE)/Basic Energy Sciences, Materials Sciences and Engineering Division under Contract DE-SC0012704. KS is supported in part by NSF under Grant No. ECCS-1307744 and the MCubed program at University of Michigan.

## References

- [1] J. Tao, K. Sun, W.-G. Yin, L. Wu, H. Xin, J. G. Wen, W. Luo, S. J. Pennycook, J. M. Tranquada & Y. Zhu, *Scientific Reports* 6, 37624 (2016)
- [2] C. H. Chen , S-W. Cheong & H. Y. Hwang, *J. Appl. Phys.* 81, 15 (1997).
- [3] P. G. Radaelli, D. E. Cox, L. Capogna, S.-W. Cheong, M. Marezio, *Phys. Rev. B* 59, 14440 (1999).
- [4] L. Brey and P. B. Littlewood, *Phys. Rev. Lett.* 95, 117205 (2005).
- [5] G. C. Milward, M. J. Calderón & P. B. Littlewood, *Nature* 433, 607 (2005).
- [6] J. Tao & J. M. Zuo, *Phys. Rev. B* 69, 180404 (2004).
- [7] C. H. Chen, S. Mori, & S-W. Cheong, *Phys. Rev. Lett.* 83, 4792 (1999).
- [8] M. Uehara, S. Mori, C. H. Chen & S.-W. Cheong, *Nature* 399, 560 (1999)
- [9] E. Dagotto, *Science* 309, 257 (2005)
- [10] J. Burgy, M. Mayr, V. Martin-Mayor, A. Moreo, and E. Dagotto, *Phys. Rev. Lett.* 87, 277201 (2001).
- [11] E. Dagotto, *Reviews of Modern Physics* 85, 849 (2013)
- [12] S. A. Kivelson, E. Fradkin & V. J. Emery, *Nature* 393, 550 (1998).
- [13] E. Fradkin, S. A. Kivelson, M. J. Lawler, J. P. Eisenstein, A. P. Mackenzie, *Annual Review of Condensed Matter Physics* 1, 153 (2010).

- [14] J. M. Tranquada, B. J. Sternlieb, J. D. Axe, Y. Nakamura & S. Uchida, *Nature* 375, 561 (1995)
- [15] V. Hinkov, D. Haug, B. Fauqué, P. Bourges, Y. Sidis, A. Ivanov, C. Bernhard, C. T. Lin, B. Keimer, *Science* 319, 597 (2008).
- [16] A. Mesaros, K. Fujita, H. Eisaki, S. Uchida, J. C. Davis, S. Sachdev, J. Zaanen, M. J. Lawler, Eun-Ah Kim, *Science* 333, 426 (2011).
- [17] C. Fang, H. Yao, W.-F. Tsai, J. P. Hu & S. A. Kivelson, *Phys. Rev. B* 77, 224509 (2008).
- [18] M. Rubhausen, S. Yoon, S. L. Cooper, K. H. Kim & S-W. Cheong, *Phys. Rev. B* 62, R4782 (2000)
- [19] Y. You & E. Fradkin, *Phys. Rev. B* 88, 235124 (2013)
- [20] J. Tao, D. Niebieskikwiat, M. Varela, W. Luo, M. A. Schofield, Y. Zhu, M. B. Salamon, J. M. Zuo, S. T. Pantelides, and S. J. Pennycook, *Phys. Rev. Lett.* 103, 097202 (2009).
- [21] K. H. Ahn, T. Lookman, A. R. Bishop, *Nature* 428, 401(2004)
- [22] M. T. Fernández-Díaz, J. L. Martínez, J. M. Alonso, E. Herrero, *Phys. Rev. B* 59, 1277 (1999).
- [23] Y. Kohsaka, C. Taylor, K. Fujita, A. Schmidt, C. Lupien, T. Hanaguri, M. Azuma, M. Takano, H. Eisaki, H. Takagi, S. Uchida, J. C. Davis, *Science* 315, 1380-85 (2007)
- [24] J. He, R. Wang, J. Gui & C. Dong, *Phys. Stat. Sol. (b)* 229, No. 3, 1145 (2002).
- [25] Y. Ando, K. Segawa, S. Komiya and A. N. Lavrov, *Phys. Rev. Lett.* 88, 137005 (2002)

[26] L. Nie, G. Tarjus, & S. A. Kivelson, PNAS 111 (22), 7980 (2014)

## Figure Captions

Figure 1. TEM dark-field image obtained at  $T \sim 280$  K shows the coexistence of two types of nanoclusters with stripe-like superlattice modulations on either the  $a$ -axis or the  $c$ -axis. The inset is an electron diffraction pattern obtained from the same area to confirm two types of nanoclusters with diffused scattering peaks showing on both the  $a^*$  and the  $c^*$  directions in the reciprocal space.

Figure 2. Two typical electron nanodiffraction patterns obtained from normal nanoclusters (a) and anomalous nanoclusters (b) in a single-crystalline domain during a scanning of the electron probe. (c) The scanning electron nanodiffraction (SEND) maps as a function of temperature from  $T = 235$  K to  $T = 296$  K. The scanning results were obtained from the same single-crystal domain in the sample; however, each map is not necessary in precise registration with any other. The blue, red and purple color codes are for the areas without superlattice structure, the SLR along the  $a$ -axis, and the SLR along the  $c$ -axis, respectively. A schematic drawing with stripe-like SL structure in the purple and red nanoclusters is beside the color scale for better interpretation of the SEND maps.

Figure 3. (a) The wave number measurements as a function of temperature from the SLRs in both the normal nanoclusters (red) and anomalous nanoclusters (green). The inset is the volume fraction of the nanoclusters (both types) as a function of temperature, estimated from the SEND results. (b) The anisotropy measurements from the normal nanoclusters and the anomalous nanoclusters, correlated to the thermal evolution of the lattice constants. The lattice constant plots were reported in Ref. 22 and the data has been provided by that research group.

Figure 4. An ELC phase diagram consisting of smectic, nematic and isotropic phases in  $\text{La}_{1/3}\text{Ca}_{2/3}\text{MnO}_3$ . SL stands for superlattice. DL stands for dislocation in the SL structures. Based on our results demonstrated here and in our previous work (Ref. 1), the driving mechanisms can be charge segregation for the electronic smectic-nematic transition, while both the charge segregation and strain can be responsible for the nematic-isotropic transition. In the nematic phase regime, the variation of the anisotropy coincides with the lattice constant variation through thermal process.

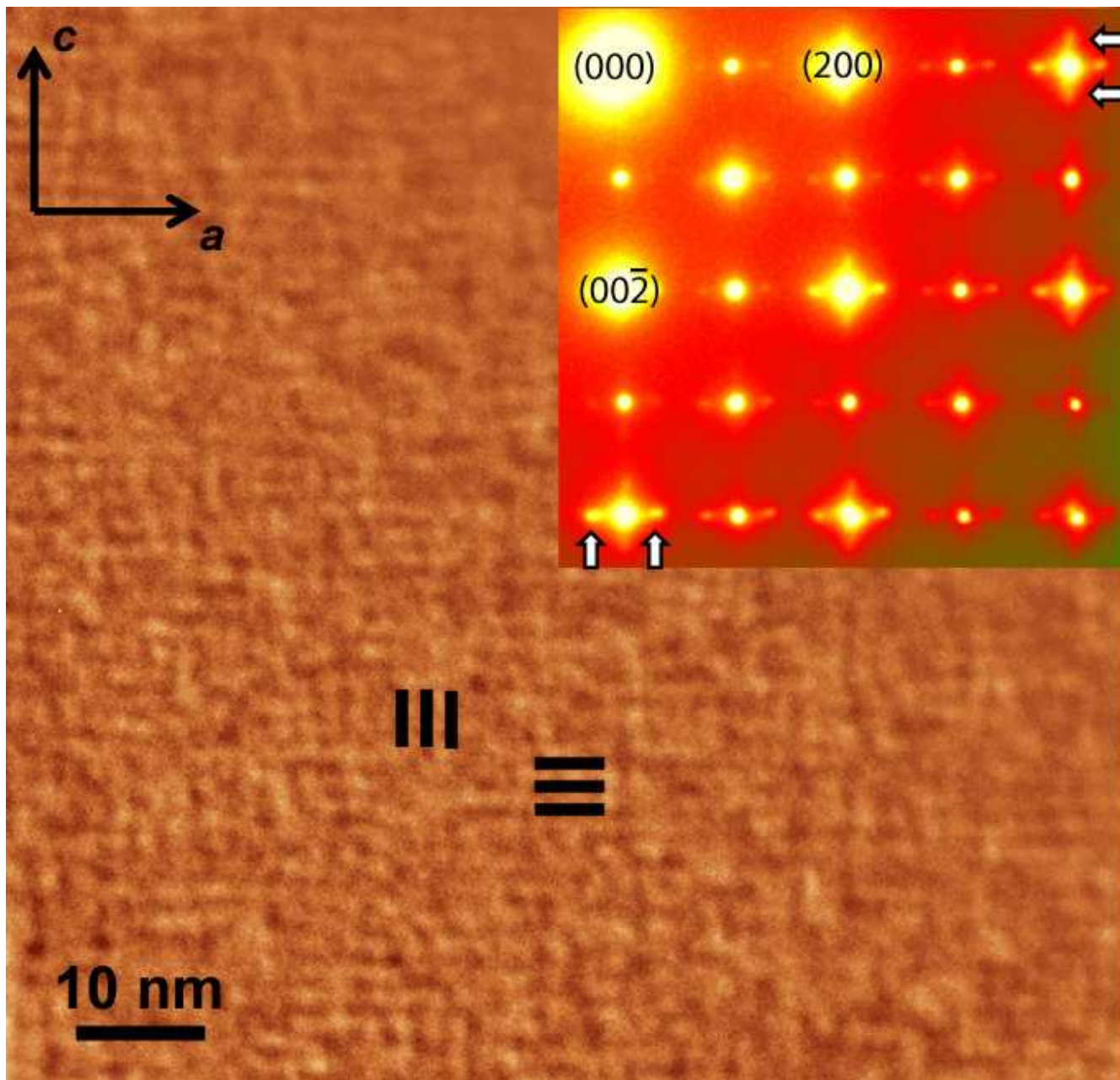


Figure 1 BB13192 12APR2017

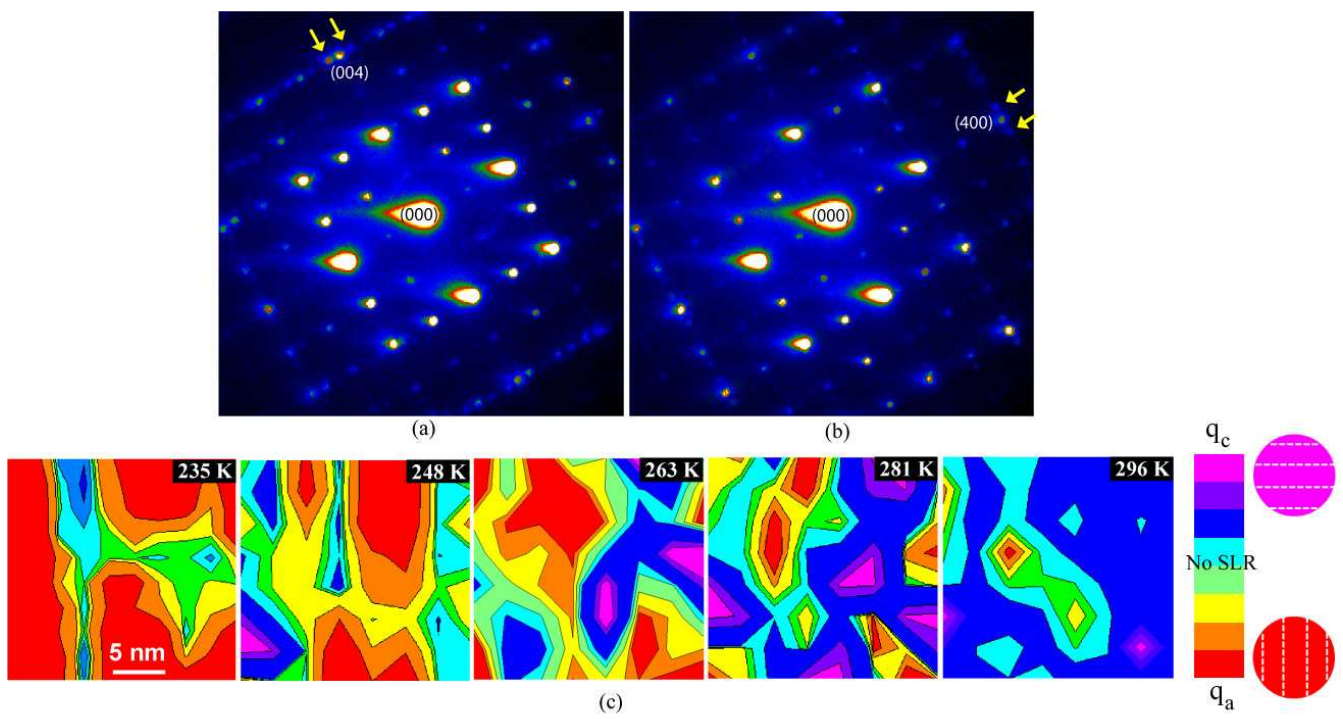


Figure 2

BB13192

12APR2017

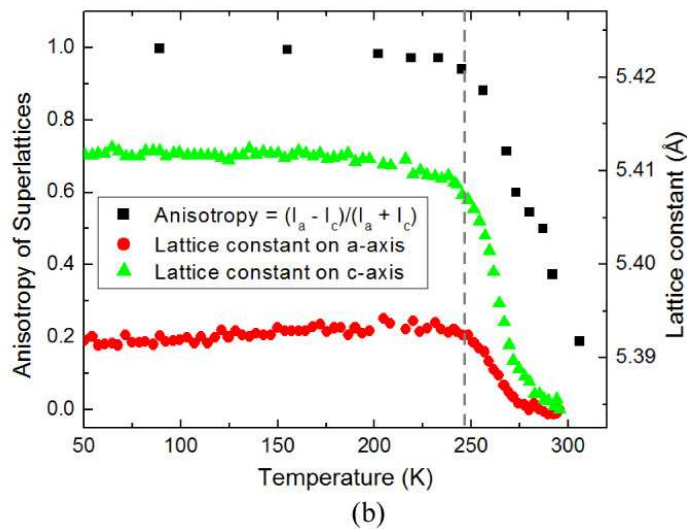
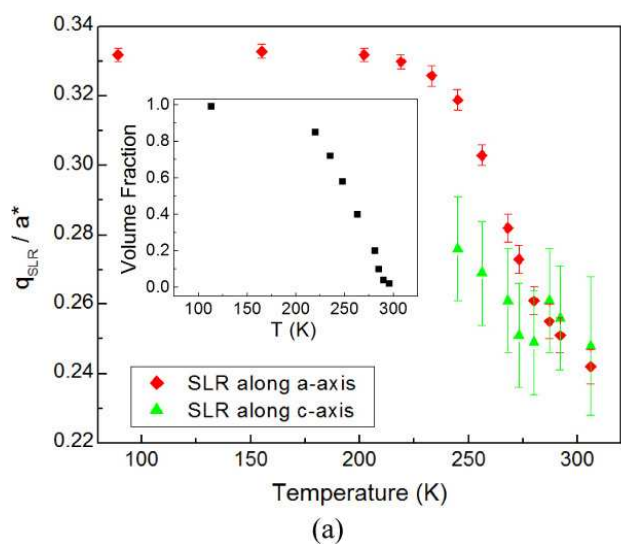


Figure 3 BB13192 12APR2017

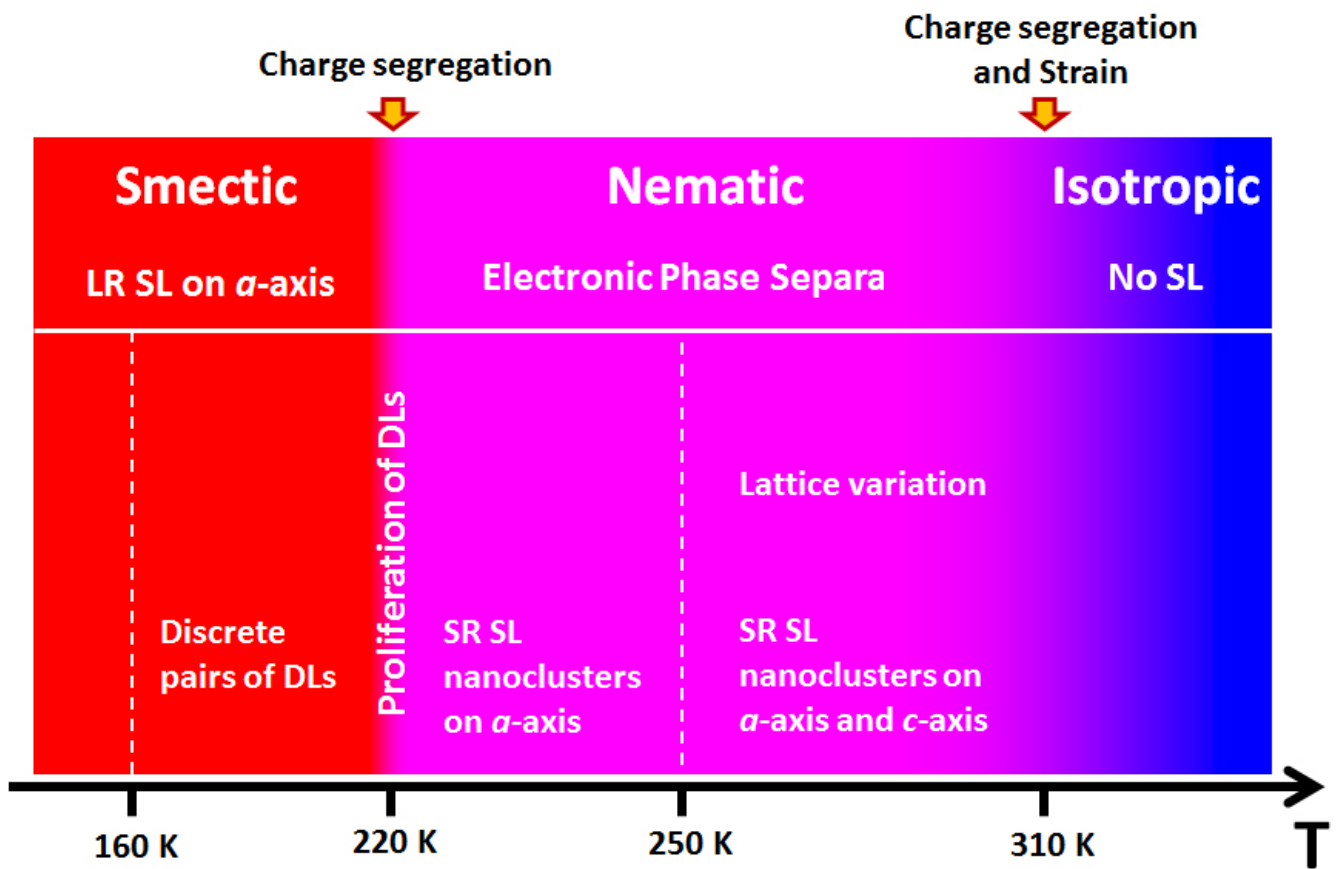


Figure 4 BB13192 12APR2017